Photochemistry at nanoparticulate surfaces

2006 J. Phys.: Condens. Matter 18 S1581

(http://iopscience.iop.org/0953-8984/18/30/S11)

INSTITUTE OF PHYSICS PUBLISHING JOURNAL OF PHYSICS: CONDENSED MATTER

J. Phys.: Condens. Matter **18** (2006) S1581–S1601 doi:10.1088/0953-8984/18/30/S11

Photochemistry at nanoparticulate surfaces

K Al-Shamery

Carl v Ossietzky Universität, Institut für Reine und Angewandte Chemie, Postfach 2503, 26111 Oldenburg, Germany

E-mail: katharina.al.shamery@uni-oldenburg.de

Received 13 January 2006, in final form 16 January 2006
Published 14 July 2006
Online at stacks.iop.org/JPhysCM/18/S1581

Abstract

Recent developments in the field of photochemistry at nanoparticulate surfaces will be reviewed. Data on laser induced diffusion, desorption and dissociation of molecules adsorbed at supported palladium nanoparticles in the size regime of a few tens to up to a few 10 000 atoms per island will be summarized. Nanosecond as well as femtosecond experiments including quantum state selective monitoring of the energy partitioning within the desorbing molecules will be presented. Interesting effects such as adsorbate induced roughening of the particles after coherent laser excitation will be reported. All phenomena exhibit a strong size dependence for the photochemistry below an average particle size of 80 Å and with remarkable changes within the population of different reaction paths below 45 Å aggregates. Defects as well as edges and kinks turn out to be important for pinning the electronically excited states.

1. Introduction

The goal of the more fundamental investigations on surface photochemistry which is the subject of this review is to get a general insight into elementary processes of bond breaking and bond making. The use of laser light enables one to study energy redistribution processes preceding bond breaking within an adsorbate in a defined way with respect to energy and time [1–7]. The concepts developed from these studies are not only important in view of the direct applications mentioned above but also contribute to our general understanding of chemical events. A deeper understanding of the relevant processes should finally enable the manipulation of chemical reactions. Classical ways to control chemical reactions include a change of temperature, pressure or the choice of a suitable catalyst to lower certain activation barriers. Laser control differs from the classical approach in the sense that active control during the course of a reaction is realized through guiding the reactants by controlling the phase of their motion [8].

In principle a direct vibrational excitation with laser light could induce bond breaking [9–12]. Here multiphoton excitation of a chosen vibration competes with vibrational

energy redistribution processes ending in phonon heating of the substrate. This effect is referred to as 'resonant heating' within the literature. It very often leads to thermal-like reactions in cases when the laser excitation pulse is much longer than the energy partitioning process.

Excitation of core electronic states normally results in different types of reaction path and is the subject of photoinduced experiments using synchrotron radiation or electron stimulated processes. For further details the reader is referred to other papers published within this special issue of this journal.

The kind of reactions this paper will deal with are induced by electronic excitation of valence adsorbate states. A direct excitation of an adsorbate valence electronic state has been found to be dominant for a selected number of adsorbate systems with rather large absorption cross sections. Mainly carbonyls and organometallics have been shown to photolyse efficiently after direct excitation [13]. Modifications of the absorption spectra from the interaction with the substrate is very often utilized in laser induced chemical vapour deposition for fabricating microelectronic devices [13].

However, there are numerous examples for which a charge carrier transfer from the substrate to the adsorbate is the relevant excitation step [1–7]. This electronic excitation is followed by transfer of energy into nuclear motion. The process will only be efficient if the system stays long enough within the adsorbate excited state for sufficient energy transfer into nuclear motion to occur [14–16]. As electronic deexcitation is rather fast on metals, desorption cross sections of UV nanosecond excitation processes are rather small (maximally 10^{-18} cm^2 for some favourable situations like NO/Pt(001) and Pt(111) at 6.4 eV, generally 1–3 orders of magnitude smaller) [17]. The situation is much better on semiconductor and insulator surfaces, for example oxide surfaces [3]. Lifetimes of excited states are at least 10 times longer, leading to much larger desorption efficiencies (by at least two orders of magnitude).

As the dominating process of a photochemically induced surface reaction is an interaction of charge carriers with the adsorbate, the first step for an optical control of a photochemical reaction has to go via understanding the coherent electron dynamics within the substrate.

The time-varying field of an ultrashort laser pulse creates a microscopic polarization at the surface which may decay either by reemission of the field, i.e. reflection, or by absorption of a photon. The free-carrier creation is a second-order process involving the absorption of the light quantum and scattering by phonons to conserve momentum. Strong Coulomb interactions between the charge carriers as well as defects and impurities may also contribute to an efficient scattering. Thus the initially coherent excitation rapidly decays, creating an incoherent, non-equilibrium distribution of charge carriers [18–20].

The phase relation between the excitation and the external field is characterized by the phenomenological optical dephasing time τ_0. In noble metals the dephasing time of bulk excitations is of the order of two to three optical cycles of the exciting light (at 400 nm (3.1 eV) the optical cycle is 1.33 fs) which represents some of the worst cases. Thus the experimental realization of a coherent control experiment is not fundamentally limited, however extremely demanding. The situation is more favourable with respect to surface states. Surface states result from the rupture of translational symmetry of an extended periodical bulk structure at the surface. Electrons have an increased residence probability within these states. If electrons occupy an initially unoccupied surface state, relaxation occurs primarily via scattering with bulk charge carriers. The scattering probability depends on the energy difference between surface and bulk states and thus the penetration depth of the surface state into the bulk. The excitation lifetime therefore is directly related to the lifetime of the bulk states. In noble metals, dephasing times of 20 times the optical cycle can be found, which is easier to handle in view of coherent control experiments than the bulk states. Furthermore, surface states can be modified by changes of the surface potential through adsorbates [22].

As nanoparticles in the small size regime are dominated by surface properties, it has to be expected that laser chemistry at nanoparticles differs much from the surface chemistry of bulk materials. Surprisingly there is little detailed knowledge on the mechanisms of how photons modify molecules adsorbed at nanostructured surfaces.

A first theoretical prediction has been given by Zhdanov and Kasemo on the enhancement of cross sections of substrate-mediated photoinduced chemical reactions on ultrathin metal films by easily a factor of 10 [23]. They suggested to use multilayer sandwich systems. In a first layer the photon-to-electron conversion can be optimized while a second layer minimizes the inelastic damping of hot electrons (i.e. maximum mean free path) and a third layer performs the hot electron induced photoreaction. The rather basic model calculations presented are performed on a simpler system consisting of an ultrathin (10–30 Å) metal film deposited on a semiconductor. The main idea is to use a metal film to activate the molecules which is thick enough to have properties of the semi-infinite metal but thin enough to permit easy passage of the externally generated hot electrons through it. The role of the semiconductor is to allow excitation of photoelectrons which will diffuse in the semiconductor over considerable distances with slow dissipation of energy and interact from time to time with the metal film. As energy dissipation will mainly occur in the metal film, the electrons will eventually be trapped in the film, generating secondary electrons. The enhancement factor roughly depends on the film thickness of the metal film and the mean free path with respect to the excitation of electron–hole pairs in the metal. Triggered by the experimental work presented in this review Zhdanov and Kasemo recently extended their theoretical work towards supported nanometre-sized metal particles [24]. They pointed out that the confinement of the electrons within the nanometre-sized particles increases the contribution of secondary hot electrons to the photochemical conversion and therefore is beneficial for an efficient photochemistry both under steady state conditions (linear regime) as well as under sub-picosecond laser pulses (nonlinear regime).

A comparable approach has been given in two earlier papers by Gadzuk, who developed a theory on resonance-assisted hot electron femtochemistry at surfaces in a solid state tunnel junction composed of metal–insulator–metal substrates [25, 26]. The difference from Zhdanov and Kasemo is that the hot electrons are supplied via field induced injection.

The early theoretical work motivated the author to perform experiments on nanostructured surfaces reviewed within this article. When one decides to enter the universe of nanoparticles, one has to be aware of the fact that such systems are far more complex than low index single crystal surfaces [27–30]. Changing to nanoparticles is not simply a change of the surface to volume ratio. Quantization effects occur for metal particles consisting of a few atoms. The electronic structure of aggregates even as large as a few hundred atoms may be simply influenced by the amount of adsorbates. For example, CO can modify the electronic structure of palladium particles of about 100 atoms from metal to more molecular-like behaviour when increasing the coverage [31]. Even rather large nanoparticles from coinage or alkali metals exhibit collective resonances of the electrons, known as plasmon resonances, which vary with particle diameter [32]. The amount of edges, kinks and defects may influence the electronic structure of the metal particles in a substantial way. Surfaces with different termination and thus different reactivity are present within diffusion lengths on small particles. Furthermore, the lattice structure of supported particles may be different from the bulk material because of the interaction with the support. If the particles nucleate at defects of the support, partial charge transfer from the defects to the metal particle may occur, depending on the nature of the defect. The perimeter between the nanoparticle and the support is a new interface with important properties. Two chemically rather different systems such as the metal particle and (very often) the oxidic support are within a close neighbourhood so that spill over may lead to a chemistry strongly depending on the composition of the hybrid system. Under ambient

conditions the particles may change their shapes because of changes in the wettability of the support triggered by the large amount of adsorbates in a much more pronounced way than single crystal surfaces. All these problems and even more have made supported nanoparticles some of the most fascinating systems of ongoing research, not only because of their immense technological importance such as in heterogeneous catalysis with which more than 80% of the basic chemicals are produced [33]. Being aware of this complexity the author has chosen to work on one type of nanoparticle/support system and vary the adsorbate systems in order to learn details about branching ratios between reaction pathways as a function of particle size after UV laser excitation. The paper therefore focuses on palladium particles with between a few and up to more than 10 000 atoms per particle with varying roughness interacting with an oxygen terminated alumina epitaxially grown on NiAl(110) [34–38]. When starting this work this was one of the best characterized systems at that time. Results on CO diffusion, NO desorption and methane photodissociation will be reviewed, including femtosecond experiments.

Principally there are two different approaches for the nanostructuring of surfaces. The technologically most important method is a top-down method, lithography (using photons or electrons), a method of immense technological importance in microtechnology. The principal lower limit is about 10–15 nm because of interference effects [13]. Related to lithography are methods by photochemically dissociating volatile precursor molecules either directly above the surface within the gas phase or as adsorbates in order to shape surfaces [13]. Diffusion is rather often a limiting factor within the fabrication of well defined nanostructures. Besides this approach there are numerous possibilities for the so-called 'bottom up' production of nanomaterials. The technologically most relevant fabrication methods are based on sol–gel methods for real catalyst productions [39]. For more fundamental investigations a number of methods based on self-assembly techniques are suitable for small-scale structuring of periodic features of sizes between 1 and 50 nm [40, 41]. Monomicellar films using block copolymer micelles or colloids are produced using Langmuir–Blodgett or related techniques. In order to produce aperiodic patterns micro-contact printing is suitable to produce patterns of down to 50 nm. The resolution is limited because of the contact stability of the stamps [42]. Other approaches use dip-pen nanolithography, i.e. the application of a molecular ink using the tip of an atomic force microscope [43], block copolymer lithography [44–47], colloidal lithography [48] and self-assembled monolayer lithography [49, 50]. Combined lithographic as well as self-assembly approaches have been successful even for producing vertical colloid device architectures [51]. First examples have been published in which bare metal particles can be obtained from such structures using plasma treatment of the monomicellar films [47, 52, 53]. Otherwise bare nanostructured surfaces in well defined arrays have been obtained applying scanning tunnelling microscopy either under UHV (to fabricate rather small sized nanoparticles consisting of a well defined number of a few atoms) [54] or as part of an electrochemical set up in solutions [55]. Soft landing of size selected clusters is a further way of nanofabrication; however, it is experimentally rather demanding [56–58].

A rather simple method is physical vapour deposition with which one is able to prepare particle sizes of between a few atoms up to a couple of 10 000 atoms per particle with rather low dispersion of the particle size [27–30, 59]. Metal atoms are deposited onto the surface. Depending on the interaction between the metal and the support, growth of nanoparticles occurs in a homogeneous or heterogeneous growth mode. In some spectacular cases terrace nucleation or regular protrusions within low index surfaces can act as nucleation centres in order to obtain astounding regular nanowires or nanodots. The beauty of the method is not only the simplicity with respect to its technique, but also the large range of rather monodisperse particles available under ultra-high vacuum conditions. Furthermore, the surface temperature may allow one to

influence the particle structure and island density. As this is actually the easiest method so far in order to obtain well defined surfaces this is the method of our choice.

2. Experimental set-up

Mainly two different ultra-high vacuum (UHV) systems ($p < 3 \times 10^{-10}$ mbar) have been used within the experiments outlined in this paper. Details of the equipment have been given elsewhere [34–38, 60].

One system was equipped with a low energy electron diffraction (LEED/Auger) optics, quadrupole mass spectrometer (QMS) for residual gas analysis and temperature programmed desorption (TPD), FT-IRRAS (Fourier transform infrared reflection absorption spectroscopy) and an ion sputtering gun. The FT-IRRAS spectra were recorded at 84° with respect to the surface normal with an optical resolution of 2 cm^{-1}. An aperture of 3.5 mm was used throughout the experiments. Background spectra and CO spectra were taken without moving the probe during the experiments. Each spectrum was scanned within three minutes and was smoothed (9-point). Background corrections were done in cases of noticeable background shifts using a polynomial fit to the slope of the broad background.

A second system was equipped with XPS, LEED (Spectaleed from Omicron) and a multichannel array for REMPI (resonance enhanced multiphoton ionization). XP spectra were recorded using non-monochromatic Mg Kα radiation and a hemispherical electron analyser (HA100 from VSW Scientific Instruments). For certain experiments particle sizes were checked with SPA-LEED.

An epitaxial film of alumina of 5 Å thickness was obtained prior to each experiment by oxidizing a clean NiAl(110) single crystal at an oxygen pressure of 1×10^{-6} mbar at 550 K. Annealing at 1130 K for 5 min leads to an oxygen terminated film [61]. The quality of the alumina film was controlled with low energy electron diffraction (LEED). A final quality test of the oxide film is the lack of CO adsorption at 120 K, which can be checked by FT-IRRAS and TPD. Pd (99.95%, Alfa) was deposited by an electron beam evaporator (tectra) onto the alumina film.

Carbon monoxide (^{12}CO, Messer, >99.9995%) was dosed via background dosing at pressures of about 10^{-9}–10^{-7} mbar. Exposures are given in Langmuir units (1 L = 1.33×10^{-6} mbar s). According to TPD data a saturation coverage of CO was obtained when dosing approximately 30 L (1 L = 1.33×10^{-6} mbar s). The preparation of the isotopic mixtures of ^{12}CO/^{13}CO (^{13}CO: 99% ^{13}C and <10% ^{18}O, Isotec) was carried out in the gas system of the UHV chamber. Partial pressures of the individual gases were determined with a Pirani pressure gauge and the adsorbed ratio of ^{12}CO/^{13}CO was checked by TDS detecting masses $m/z = 28$ and 29.

Nanosecond laser experiments on CO diffusion were carried out using a frequency tripled Nd:YAG laser (Spectra Physics, Quanta-Ray GCR 130) at 355 nm with a repetition rate of 10 Hz and with maximally up to 10 mJ cm^{-2} per pulse (pulse length: 8 ns). Laser experiments on NO desorption and methane dissociation were performed using 15 ns pulses of an excimer laser impinging normal to the surface at three different wavelengths (3.5, 5.0, 6.4 eV). Femtosecond experiments were performed with laser pulses of a diode laser pumped Ti:sapphire laser which was amplified within a regenerative amplifier yielding pulse lengths of 70 fs at $\lambda = 400$ nm with 120 mW cm^{-2} and a repetition rate of 700 Hz. The excitation energy is well below the band gap of alumina.

A tunable detection laser (excimer pumped dye laser) for recording NO spectra was fired at a time delay with respect to desorption which defined the flight time of the molecules after desorption into the detection area. Time of flight spectra for single rovibronic states were

obtained by varying the time between desorption and detection and averaging over 300 pulses per delay. The spectra were then transformed into velocity flux distributions taking the distance of the surface to the detection volume into account. Tuning the wavelength of the detection laser run at a fixed time delay resulted in desorption spectra giving the final state distributions for a defined desorption velocity of the molecules. As a detection scheme, REMPI was used to ionize the molecules. For NO a REMPI (1, 1) scheme via the $A^2\Sigma$ state was chosen [62]. The ions were detected with a unit consisting of a repeller, a short flight tube, multichannel plates and a phosphor screen.

To keep a steady state coverage during the experiments the molecules were dosed to the surface via a background pressure of 5×10^{-8}–2×10^{-7} Torr. Liquid nitrogen cooling kept the temperature of the surface at 100 K.

3. Results

3.1. Sample preparation

Within the work presented 0.04–1.2 nm Pd (nominal thickness obtained by a calibration with a quartz microbalance, tectra) was deposited at 120 or 300 K onto an epitaxial alumina support (grown on NiAl(110)) with an electron beam evaporator. Pd aggregates nucleate at defect sites of the alumina as described by Bäumer *et al* [63]. Deposition of palladium at 100 K leads to highly dispersed aggregates with amorphous structure. Cubooctahedral ordered structures with mainly (111) terraces and a minority of (100) terraces are obtained when growing the aggregates at 300 K [64].

According to the work of Bäumer, Libuda and Freund the deposited amount of palladium will lead for example to average aggregate sizes of 100 atoms per island with rough surfaces (0.2 nm deposited at liquid nitrogen temperature, island density of 1.4×10^{13} cm^{-2}), 2000 atoms per islands with rough surfaces (1.0 nm deposited at liquid nitrogen temperature, island density of 0.4×10^{13} cm^{-2}), 2000 atoms per island with dominating (111) ordered terraces (0.2 nm deposited at 300 K, island density of 0.1×10^{12} cm^{-2}) and 6000 atoms per island with ordered, dominating (111) terraces (0.6 nm deposited at room temperature, island density of 1.0×10^{12} cm^{-2}). As the island density depends on the defect density the process is rather reproducible, as checked with SPA-LEED and STM in different UHV chambers with various NiAl samples. Under the same oxidation conditions of the NiAl the same amount of defects can be found. A certain overall roughening has to be noted of the NiAl crystal during femtosecond laser experiments which is also apparent from LEED. It is to be expected that the concomitant density of defects in the alumina film is increased with respect to an untreated crystal. Therefore the actual aggregate sizes might be smaller and the density higher than the data given. This trend is also apparent from the IR spectra of the CO stretching vibration which are rather sensitive to the aggregate sizes and the ordering of the aggregates. The numbers given for the average aggregate sizes therefore have to be seen as upper limits. The key statements of this paper, however, are unaffected.

3.2. Laser induced diffusion

3.2.1. CO/Pd-nanoparticles/alumina/NiAl(110). CO adsorption at Pd particles grown on epitaxial alumina/NiAl(110) is rather complex in comparison to flat single crystal surfaces. Sandell *et al* found that the electronic properties of the whole CO–Pd complex is strongly dependent on the island size and CO coverage using combined x-ray photoelectron spectra, x-ray absorption spectra and core–hole decay techniques [31]. Even for islands containing 100 Pd atoms, the screening ability of the aggregate is reduced for large amounts of CO adsorbed and

can even exhibit small effects of molecular carbonyl-like systems. This will be due to the formation of discrete molecular orbitals rather than a continuous band because of the $2\pi^*$–d interaction, if the CO/Pd ratio is of the same order as for carbonyls. On the other hand, for low coverages of CO (i.e. half of a saturation coverage) relaxation of core ionization is nearly as efficient as for metallic systems. Even bare metal particles as small as 10 atoms can exhibit metallic-like screening behaviour.

Furthermore, CO adsorption at Pd particles is influenced by the large amount of edge and kink sites as well as by the coexistence of particle facets in different terminations [65, 66]. A stepped Pd(112) surface has close similarities to the cubooctahedral Pd aggregates. It consists of three-atom-wide terraces of (111) orientation, separated by monatomic steps of (001) symmetry. ESDIAD (electron stimulated desorption ion angular distribution) measurements on this surface by Ramsier *et al* [67] and our own measurements [68] with FT-IRRAS revealed that preferential adsorption takes place first at the step sites with no evidence for CO tilt directions parallel to Pd step edges. At higher coverages terrace and step CO coexist. The data indicate that CO dissociation occurs at low coverages at 120 K at the step sites [68]. This is the first report on CO dissociation at a palladium surface. At room temperature, CO recombines because of a higher mobility of the fragments. At the nanoparticles there is no indication for CO dissociation in substantial amounts before or during laser irradiation.

The local electron density distribution and the local electric field strengths at the surface are expected to be highly anisotropic at such stepped surfaces. The overall charge transfer within CO bonding creates an electric dipole at the step which explains a higher degree of short-range CO–CO interactions at stepped surfaces compared to a flat surface as is evident from TPD [67, 68].

Wolter *et al* investigated the CO adsorption at nanosized Pd particles in FT-IRRAS studies [65, 66]. They assigned the observed vibrations to occupied bridge sites on terraces and edge sites and occupied on-top sites for a saturation coverage, which is less dense than at the Pd(111) surface. Considering recent findings the author follows the assignment accommodating the preference of three-fold site occupation at (111) terraces and the development of higher adsorbate densities in domain walls also existing at small Pd particles. Tüshaus *et al* pointed out that on Pd(111) single crystals this implies the formation of regular streaks of domain and antiphase domains, also called 'solitons' within the literature [69]. With the help of the domain wall model it is easier to appreciate that the structures represent a compromise between the lateral repulsion, which favours hexagonal close-packing, and the surface–molecule interaction, which favours site-specific adsorption [69, 70]. Actually these domain walls became visible in STM studies in the groups of Sautet *et al* (CO/Pd(111), $T = 120$ K [71, 72]) and Besenbacher (CO/Pt(111), $T = 300$ K [73]). Whereas CO occupies three-fold fcc and hcp sites for low coverages up to $\Theta = 0.33$, the interpretations of the adsorbate geometry for $\Theta = 0.4$ to 0.6 vary between phase transitions from three-fold to bridge site adsorption or an overall favoured adsorption structure in three-fold geometry. However, the STM experiments of Salmeron *et al* revealed that islands in three-fold geometry as well as islands in bridge site geometry are existing parallel for intermediate CO coverages [71, 72]. Additionally, transitions from three-fold to distorted bridge site adsorption within one domain with simultaneous changes of domain wall geometries were detectable. At saturation coverage the CO molecules occupy three-fold fcc and hcp sites in hexagonal geometry with an on-top CO molecule in the centre of this arrangement.

Different adsorption sites can also be monitored using IR spectroscopy of the intermolecular vibration of CO. CO bonding results from CO-5σ to metal donation, metal-d-band to CO-$2\pi^*$ backdonation and metal substrate polarization [74, 75]. The adsorbate levels mix with the states of E_F of the substrate due to hybridization with the metal d-band.

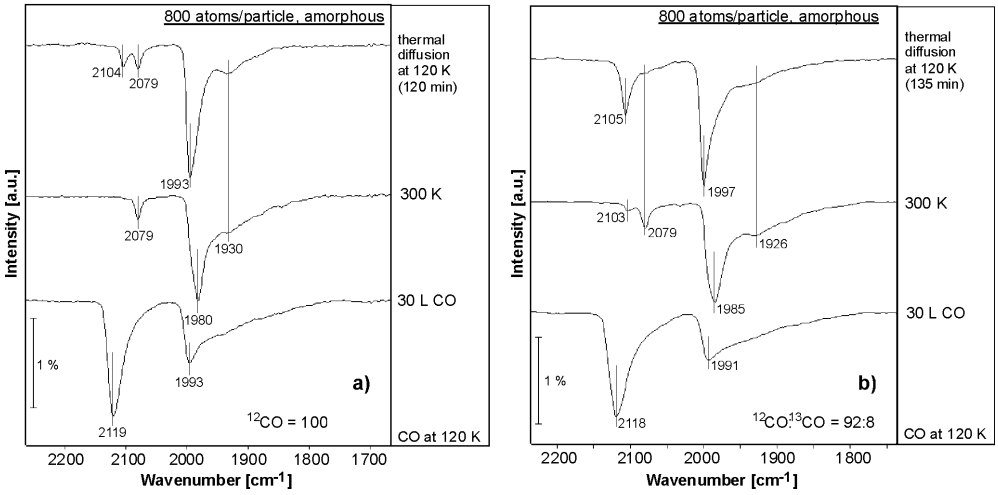

Figure 1. Two sets of IRA spectra of (a) ^{12}CO and (b) an isotopic mixture containing ^{12}CO/^{13}CO 92:8 at amorphous Pd particles of 800 atoms average size. Saturation coverage (bottom), after annealing the saturation coverage to 300 K for 10 s and subsequent cooling to 120 K (middle) and after a diffusion time of (a) 120 and (b) 135 min (top) [77].

As a result the intermolecular stretching vibration in the CO molecule varies with the amount of backdonation depending on the adsorption geometry. But simple attribution of vibrational frequencies to distinct adsorption sites is complicated by coverage dependent surface–molecule and molecule–molecule interactions. Competitive backdonation from the metallic surface to the $2\pi^*$ molecular orbitals of neighbouring CO molecules and dynamic vibrational coupling between adsorbate molecules can lead to strong frequency shifts for a considered adsorption site from $\Theta \rightarrow 0$ to saturation coverage. In the case of CO/Pd(111) an IR absorption band at about 1850 cm^{-1} at low coverage can be detected which shifts to higher values with increasing coverage [76]. For intermediate coverages between $\Theta = 0.5$ and 0.6, IR absorptions between 1920 and 1979 cm^{-1} are visible. At saturation coverage the IR spectrum shows two absorption features with nearly identical intensities at 1894 cm^{-1} (three-fold site) and 2110 cm^{-1} (on-top site).

As will be discussed further below, laser induced redistribution processes of adsorbate sites are observed when preparing non-equilibrium CO coverages. However, before tackling laser induced dynamics one first has to deal with the problem that thermal induced diffusion may occur for such non-equilibrium coverages. Different CO adlayers have been prepared for this purpose at nanosized Pd particles at 120 K by short annealing of a saturation coverage to 300 K with subsequent cooling to 120 K. This annealing temperature results in a nearly complete depopulation of on-top adsorption species.

How do such coverages differ from coverages obtained under thermodynamical equilibrium conditions? As was discussed, islands or domains are built at Pd(111) and Pt(111) for CO adsorption at high coverages [71–73]. Intermolecular attractive or repulsive interactions can affect the diffusion resulting in such islands. Experimental and theoretical studies have shown that the domain boundaries of the adlayer can be thermally very stable in comparison to the more open adsorbate structures obtained under thermodynamic equilibrium conditions due to strong intermolecular interactions.

Figure 1 shows the FT-IRRAS spectrum of the CO stretching vibration of isotopically pure and mixed CO coverages for an intermediate particle size of 800 atoms per island grown

at 120 K. Two general effects are detectable with infrared reflection absorption spectroscopy: first an isotope dependent reoccupation of on-top adsorption sites and second a restructuring of the multiple bonded CO adsorbate (decrease of signal 1930 cm^{-1} (three-fold hollow site), increase of edge site and signals of Pd(100) sites at 1997 cm^{-1} and increase of the regular on-top site feature at 2105 cm^{-1}). For a pure ^{12}CO adsorbate compressed adsorbate structures at domain boundaries in three-fold coordination exhibit stabilizing attractive interactions along the domain walls. A disturbance of the adlayer by even a low amount of ^{13}CO molecules (by less than 10% of the overall coverage) leads to a generally enhanced diffusion. A stronger depopulation of three-fold adsorbed molecules in compressed adsorbate structures is induced by ^{13}CO molecules in comparison to a pure adlayer. Both effects are influenced by the (i) particle morphology and (ii) particle size. These experiments on isotopic mixtures of $^{12}CO/^{13}CO$ revealed that dipole–dipole interactions play a crucial role for stabilizing compressed adsorbate structures [77]. A disturbance of intermolecular coupling by ^{13}CO isotopes results in a decrease of intermolecular attractive forces. In applying infrared reflection absorption spectroscopy to these Pd particles, one has to consider infrared selection rules. At metal surfaces only dipole moments perpendicular to the surface are detectable. Therefore adsorbed molecules at the side facets of the particles with a dipole moment predominantly parallel to the surface are underestimated within the infrared spectra. Otherwise, due to long-range dipole–dipole interactions these molecules can influence the vibration of molecules adsorbed at the top terraces showing the main absorption signal.

Hence it is difficult to distinguish between molecules diffusing intrinsically at the top face or diffusing over face boundaries from site facets to top faces. The data however indicate that diffusion over communicating facets should be taken into account. Indications are an increase of the overall IR intensity and the narrowing of the band at 1996 cm^{-1} (readsorption from residual CO in the gas phase could be excluded). The latter indicates a higher occupation of two-fold edge sites at the particles resulting in stronger dipole–dipole coupling. Such a concentration process at defect sites is well known in surface diffusion [78]. At crystalline particles with smooth particle facets the energy is sufficient to induce diffusion over the facet boundaries to the top facet.

Another point found in the experiments is the particle size dependence of the effects of CO diffusion. Amorphous particles of 100 and 800 atoms per particle average size exhibit a decrease in on-top site reoccupation with increasing particle size. Accompanied with this decrease are the changes of the absorption band of two-fold adsorbed molecules at edge sites with regards to the discussion above. With increasing particle size the size of the particle facets grows, too. Assuming a constant diffusion length for CO molecules at 120 K at amorphous particles it is obvious that with growing particle facets the probability for crossing the facet boundary to the top face must decrease.

Furthermore it has to be noted that an Ehrlich–Schwoebel barrier makes diffusion up and down a step direction dependent. In the case of Pd particles there are mainly (111) and (100) facets at the particle sides. One therefore has to deal with two different steps separating those facets with the topmost (111) facet. Transport between those facets may not be equally probable. Therefore the amount of a certain type of steps with increasing particle size may be relevant as well.

As a rough estimation the diffusion activation energy of an adsorbed species is about 25–30% of the adsorption energy. The desorption energy of three-fold coordinated ^{12}CO molecules at large crystalline particles (8000 atoms per particle average size) is 128 kJ mol^{-1} [37]. So one can estimate a diffusion activation energy of 32–38 kJ mol^{-1}. The fact that by applying a distortion with ^{13}CO molecules three-fold adsorbed species can diffuse, the forces, which stabilize the compressed structures, must be at least in the range of 30 kJ mol^{-1} at 120 K.

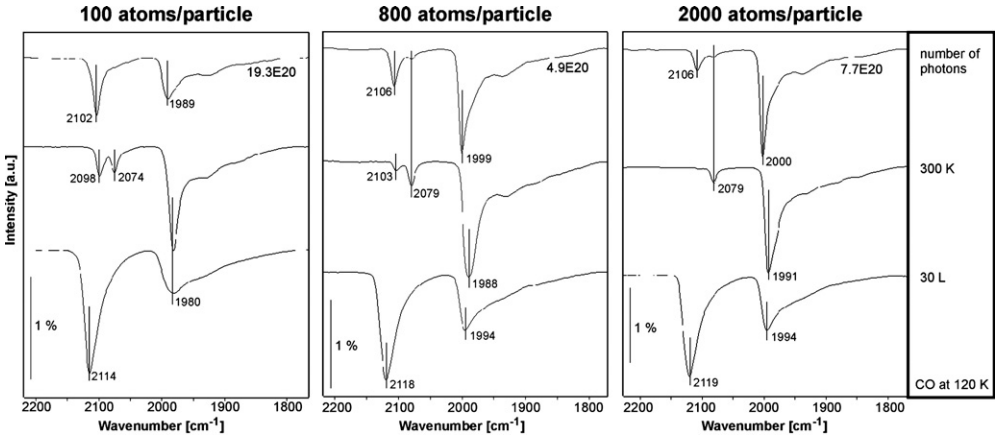

Figure 2. Sets of FTIR spectra for three different amorphous aggregate sizes (100 atoms/island, 800 atoms/island, 2000 atoms/island): saturation coverage (bottom curves), spectra after annealing to 300 K (middle curves), final state of the laser experiment after impinging the number of photons onto the surface as indicated (upper curves); all spectra recorded at 120 K.

3.2.2. Nanosecond experiments. No laser activity is observed when irradiating a normal coverage of CO adsorbed via background dosing palladium particles. In contrast to CO/Pt ESDIAD studies [79], the lack of desorption of neutral, electronically excited CO may be explained by preferential CO bonding to hollow sites on Pd while CO prefers terminal bonding on Pt. In a hollow site position CO experiences a higher quenching probability and a lower cross section for initial excitation due to a larger amount of metal-electron backdonation in contrast to terminal or bridging CO.

However, the situation changes when irradiating metastable non-equilibrium coverages of CO at the palladium particles with a Nd:YAG laser at $\lambda = 355$ nm [37]. Such coverages are obtained via tempering a saturation coverage to 300 K. This is apparent in figure 2, exhibiting the FT-IRRAS spectra of the CO stretching vibration of palladium particles covered with CO at about 50% of a saturation coverage before and after laser irradiation for three different particles. As is apparent from figure 2, laser enhanced depopulation of CO from three-fold hollow sites, (100) terrace sites and/or edge sites is dominant (1930–1990 cm^{-1}) and to some extent laser induced repopulation of initially depopulated on-top sites (2072–2118 cm^{-1}). The laser induced adsorption site changes of CO are correlated to the presence of higher local adsorbate densities and/or substantial population of edge sites and occur in a very narrow coverage regime of CO at rough and ordered particles up to 7000 atoms per island. It starts when the IR intensity ratio of the CO stretching vibrations is approximately 1:4 (on-top:higher coordinated sites) and ends at a ratio 1:1. The redistribution can be reversed by thermally heating the system to 230 K, as shown in figure 3. Readsorption of CO from the gas phase could be excluded. For the largest particle size investigated only shuffling of local adsorbate density fluctuations (apparent from shape changes of vibrational features around 2000 cm^{-1}) has been observed but little to no repopulation of on-top species.

As was pointed out in the introduction, UV laser induced processes on metal surfaces quite often start with an electronic excitation of metal electrons which then can interact with the adsorbate system provided that the absorption cross sections of the adsorbates are not very pronounced. Within the most simple model, the MGR model (Menzel–Gomer–Redhead), the molecule is accelerated away from the surface within the excited repulsive state [14, 15]. After a normally rather short lifetime the electron is transferred back to the substrate, setting the

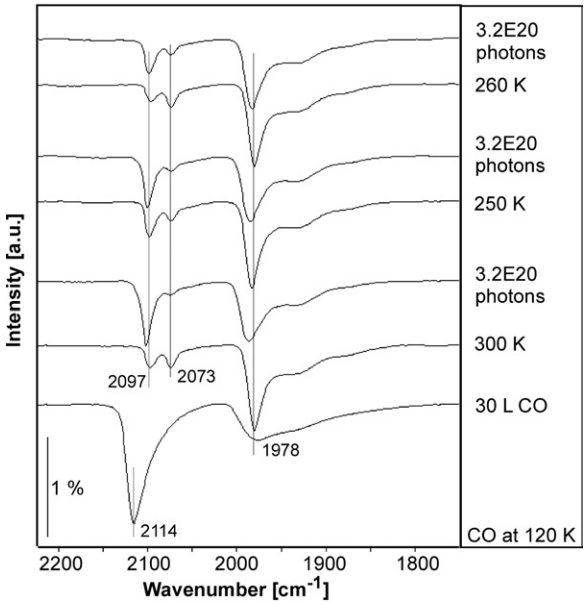

Figure 3. Cycles of tempering and laser experiments (temperatures and number of photons impinged onto the surface as indicated) of CO/Pd/alumina (∼100 Pd atoms/island) starting with a full saturation coverage (30 L) at 120 K [37].

molecule into its electronic ground state. If the molecule gains enough kinetic energy within the excited state it will desorb. Otherwise it remains on the surface normally vibrationally excited. If the vibrational excitation is large enough, hopping of the molecule may be a result of the energy exceeding the diffusion barrier. Coupling within areas of increased adsorbate density is apparently crucial for the hopping, as has also been shown for thermal diffusion of chains of CO at Cu(110) [80].

3.2.3. Femtosecond experiments. Femtosecond excitation of metastable CO coverages opens new reaction paths, as shown in experiments on CO adsorbed at Pd aggregates between 100 and 6000 atoms per island using femtosecond pulses of laser light at $\lambda = 400$ nm with pulse lengths of 70 fs [38]. Laser induced desorption of CO and H_2 dissolved within the palladium aggregates is observed for small aggregate sizes when using femtosecond laser pulses in contrast to nanosecond experiments. Efficiencies for CO diffusion are up to eight times larger for femtosecond experiments compared with nanosecond experiments and are largest for intermediate aggregate sizes (around 2000 atoms per island) for the aggregates investigated. In contrast to nanosecond experiments adsorption site populations beyond the thermal equilibrium can be observed, as is apparent from FT-IRRAS spectra of the CO stretching vibration shown in figure 4. Strong laser population of on-top sites (vibrations around 2100 cm^{-1}) goes in hand with a roughening of the aggregate surfaces and even partly with decomposition of the aggregates which has not been noticed for nanosecond experiments. This may be concluded from the formation of carbonyl-like palladium atoms for intermediate sized particles which is apparent from the observation of a vibrational feature at 2032 cm^{-1}. Such carbonyl species are only observed for aggregates consisting of only a few atoms. Though the effect is less pronounced for particles as large as 6000 atoms per island, a certain degree of surface roughening has still to be noticed from irreversible changes within the IR spectra. The

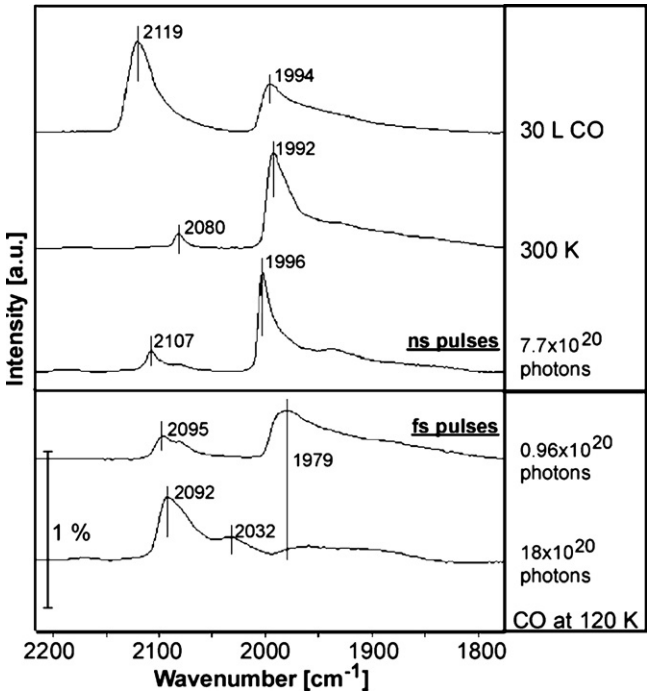

Figure 4. Sets of FTIR spectra for an average of 2000 atoms/island, grown at 120 K of the CO stretching vibrational region. Lower three curves: saturation coverage of CO (30 L, top curve), spectrum after annealing to 300 K for 30 s (second curve) and final state of a nanosecond laser experiment ($\lambda = 355$ nm, 10 Hz). Upper curves: two selected curves from femtosecond experiments: 1.8×10^{21} photons and 9.6×10^{19} photons (400 nm, 70 fs, 120 mW cm^{-2}, repetition rate of 700 Hz) impinged on a saturation coverage of CO (30 L) tempered to 300 K for 30 s prior to the laser experiment [38].

roughening is clearly correlated to non-equilibrium coverages of CO exhibiting larger densities of CO molecules at edge sites and/or elevated local adsorbate densities. The same overall coverage, however, obtained via background dosing at liquid nitrogen temperature does not lead to particle roughening neither with nanosecond laser pulses nor with femtosecond laser light.

In order to understand the experimental findings, one may assume that the laser induced processes are preceded by an electronic transition likely to be a temporal palladium–CO charge transfer. Such a process has been found for a large number of similar cases and may result in vibrational excitation of the adsorbate within various vibrational degrees of freedom as mentioned above. It is furthermore known that adsorbate vibrations, particularly low frequency vibrations, can efficiently couple to lattice phonons of the underlying support. This explains why 'resonant heating' is observed when resonantly exciting adsorbate vibrations with infrared laser light [9–12]. For a number of systems the use of femtosecond laser pulses resulted in enhanced efficiencies of photochemical processes and was attributed to multiple excitation–deexcitation processes (DIMET [81]) within the duration of a laser pulse or enhanced friction creating highly vibrationally excited adsorbates [82]. Energy then may be channelled along chains of adsorbate solitons via dipole–dipole coupling followed by a subsequent trapping at certain aggregate sites within the course of the process. An efficient coupling to aggregate phonons then creates local hot spots sufficient to induce palladium atom migration. When

the size of the aggregates grows the amounts of areas with elevated local adsorbate densities may increase. On the other hand the damping of electronically excited states localized at the surface is more efficient with growing aggregate size. Therefore an intermediate size of the aggregates exhibits the most efficient surface roughening. The temperature jump within the bare particle induced by the laser pulse can be estimated to be less than 10 K for femtosecond laser pulses [24, 38] and cannot account for palladium migration.

Why may edge sites be important for the formation of hot spots? Calculations on stepped surfaces show that the occupancy of the d-band is increased and the sp-band occupancy is decreased at the upper step edge while the opposite is found at the lower step corner [83]. The overall charge transfer within CO bonding creates an electric dipole at the step, the upper step being positive and the lower edge negative. This explains a higher degree of short-range CO–CO interactions at stepped surfaces compared to a flat surface. So trapping of the excited adsorbate vibrations may be most efficient at the edges. It is interesting to note that a further condition for laser roughening to occur is the limited size of the nanoparticles. No laser induced processes either with nanosecond or femtosecond lasers have been observed for stepped surfaces such as Pd(112) under comparable conditions.

3.3. Laser induced desorption

In order to understand how an initial electronic excitation is transferred into nuclear motion followed by subsequent energy partitioning to a variety of vibrational degrees of freedom the next step is to investigate the bond fission of the molecule/surface bond. Quantum state resolved experiments on molecules desorbing into the gas phase reveal how much energy is partitioned into different rovibronic degrees of freedom within these fragments. The reason for this approach is that rovibrational excitations within very small molecules exhibit radiative lifetimes up to milliseconds within the different degrees of freedom when desorbing under collision free conditions. Experimentally this is less demanding than monitoring energy redistribution processes within the picosecond time regime on a surface. Furthermore the experiments are much more sensitive and therefore allow a very detailed mapping of the processes. Information may be obtained on translational, rotational, vibrational and electronic excitations for a variety of desorbing fragments as well as angular distributions and even alignment of the rotational axis within the laboratory frame [21, 84, 85].

Looking at the list of molecules investigated on a variety of substrates, the studies in the past were mainly focused on UV laser induced desorption of NO (2/3 of all publications). The rest was mainly (with a few exceptions) concentrated on CO. This is not just a coincidence. The reason is that desorption cross sections of UV nanosecond excitation processes are rather small on metals (maximally 10^{-18} cm^2 for some favourable situations like NO/Pt(001) and Pt(111) at 6.4 eV [17], generally 1–3 orders of magnitude smaller).

For example, in the case of a desorption cross section of 10^{-18} cm^2 using 1 mJ cm^{-2} at 6.4 eV therefore leads to desorption of approximately 0.1% of the initial coverage, i.e. roughly 10^{12} molecules desorbing from a monolayer distributed over some hundreds of rovibronic states and each with a certain velocity out of a distribution of velocities. Anyway, in order to be able to detect single rovibronic states a minimum number of molecules is necessary. For systems like NO or CO approximately 10^5–10^6 molecules per state (i.e. 10^{-10}–10^{-9} of a monolayer) are still easily detectable within a cubic centimetre. The spectroscopy of many other molecules is either much less sensitive or the spectroscopy is barely understood, like for one rather important molecule in surface chemistry, i.e. O_2.

This fact motivated us to study the laser induced desorption of NO from palladium nanoparticles adsorbed at an epitaxial alumina film.

3.3.1. NO/Pd-nanoparticles/alumina/NiAl(110). The adsorption of NO at single crystals is dominated by the strong repulsive interaction of NO. At low index surfaces NO adsorbs initially at higher coordinated sites changing to more weakly bonded on-top sites for larger coverages. Sudden changes in the adsorption energy result from changes of the distances between NO molecules (for example from second nearest to nearest neighbours) and are connected to the highly repulsive interaction of neighbouring molecules [86].

NO adsorption at nanosized Pd aggregates differs substantially from adsorption at single crystal surfaces [35]. On Pd aggregates NO bonds exclusively to on-top sites at aggregates smaller than 75 Å in diameter. Binding energies are found to be similar to binding energies of the on-top species adsorbed at low index single crystal surfaces (0.72 eV $\pm$ 0.03 eV). Besides this known on-top species a further even weaker adsorbate site has been observed at small Pd particles. It is the dominating species at the smallest aggregates. Amorphous aggregates show a larger amount of weakly bound species as compared with ordered aggregates of the same size. This indicates that an increased ratio of defect states to regular sites with decreasing aggregate size accounts for the occurrence of this weakly adsorbed species. Detailed studies of the adsorption of NO by means of FT-IRRAS, TPD and XPS are discussed in the paper by Kampling *et al* [35].

Substantial dissociation of NO occurs at elevated temperatures >350 K as has been concluded from TPD spectra as well as XP spectra of the N 1s signal. A disproportionation reaction favours the thermal desorption of N-containing species such as NO, N_2 and N_2O [35]. No O_2 or NO_2 has been detected, implying solvation of the remaining oxygen within the palladium. The ratio between the reaction product N_2 and undissociated NO increases with increasing aggregate size up to 80 Å for a saturation coverage of NO deposited at 100 K. While no dissociation of NO has been reported for low index Pd single crystal surfaces thermally induced population of edge sites initiates dissociation on stepped surfaces like Pd(112) [87, 88]. As aggregates exhibit a large amount of edge sites it can be concluded that the edge sites of the aggregates are particular important for the thermal dissociation.

However, there is no indication for laser induced dissociation when working at liquid nitrogen temperatures.

3.3.2. Nanosecond laser induced desorption. The UV laser-induced desorption of NO has been systematically studied by means of REMPI for detecting the desorbing molecules' quantum state resolved after excitation with nanosecond laser pulses at 6.4 eV as a function of aggregate size and morphology for defined nanostructures of Pd aggregates with average sizes between 5 and 80 Å. In contrast to single crystals, desorption of intact NO molecules has been observed for small aggregates of 80 Å and below. Quantization effects are known only to occur for very small aggregates consisting of a few atoms for metals. In the case presented the largest aggregates for which desorption of NO is detectable are as large as up to about 10 000 atoms per aggregate. However, the medium aggregates investigated here have dimensions smaller than the mean free path of the electrons and have a large number of surface atoms with respect to bulk atoms. The desorption efficiencies increase with decreasing aggregate size by one order of magnitude in the size regime under investigation. For aggregates with a diameter of 80 Å, the desorption cross sections are at the detection limit of our experimental set-up. Dominantly a weakly bound species desorbs.

3.3.3. Energy partitioning after nanosecond laser excitation. Elaborate quantum state resolved measurements on the UV laser induced desorption of NO from palladium aggregates on epitaxial alumina give insight into the desorption process.

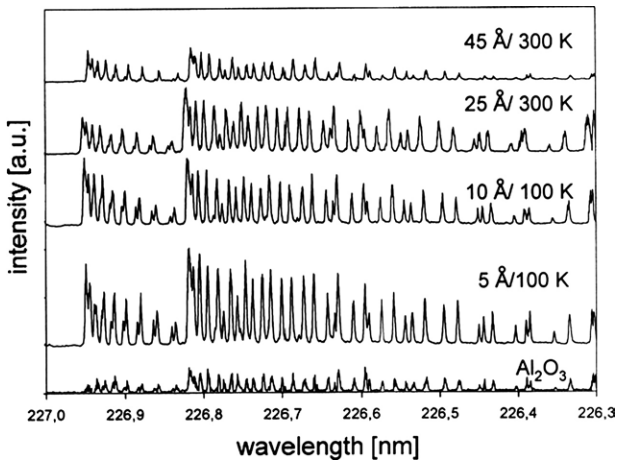

Figure 5. Overview of part of the (1 + 1)-REMPI spectra of NO (via the $A^2\Sigma$-state) desorbing from the defect sites of the pure Al_2O_3 and from different sized palladium aggregates (total amount of Pd deposited according to microbalance: at $T = 100$ K: 0.2 Å (aggregate size 5 Å); 0.5 Å (aggregate size 10 Å); at $T = 300$ K: 0.5 Å (aggregate size 25 Å); 2 Å (aggregate size 45 Å)); $v'' = 0$, $v = 1000$ m s^{-1}, $h\nu = 6.4$ eV; the part of the spectrum depicted shows part of the transitions from the $^2\Pi_{3/2}$-state [35].

Figure 5 gives an overview of part of the (1,1)-REMPI spectrum of NO from defects of the pure alumina as well as from selected palladium nanoaggregates of various particle sizes and morphology for a fixed time delay between desorption and detection, i.e. for a fixed velocity of 1000 m s^{-1}. A selected number of velocity flux distributions calculated from the recorded time of flight spectra as a function of rotational quantum number of desorbing NO is given in figure 6 for Pd aggregates of an average size of 45 Å deposited at 300 K. The velocity flux distributions are non-Maxwell–Boltzmann distributions. Analysis of the rotational temperature of desorbing NO as well as the observation of vibrationally excited NO indicates that the excitation process has to be non-thermal. Rotational temperatures between 270 and 630 K can be found which are well above the surface temperature of 100 K [35]. Such rotational temperatures are rather typically found for UV laser induced nonthermal desorption from metal surfaces. One would expect changes of lifetimes of electronically excited states and shapes of the potential energy surfaces as a function of aggregate size which would result in changes in the final state distributions. In view of the strong changes of the desorption cross sections as a function of particle size, changes within the energy partitioning as a function of particle size are, however, rather small. More surprisingly the energy partitioning, for example within the rotational degrees of freedom of the more weakly bound species, is rather similar compared with the chemisorbed species. Similarities in final state distributions have mainly been detected for aggregates with diameters below 45 Å which is of the order of magnitude of the mean free path of electrons in metals at an excitation energy of 6.4 eV.

Three different desorption mechanisms are equally likely and in accordance with the experimental observations.

(1) Desorption from low coordinated Pd atoms. One possible explanation is that desorption occurs predominantly from defect-like sites (edges, kinks, defects). For such a site the electronic structure is strongly localized and therefore little affected by the overall electronic structure. This would result in similar lifetimes of the excited state and thus similar final state

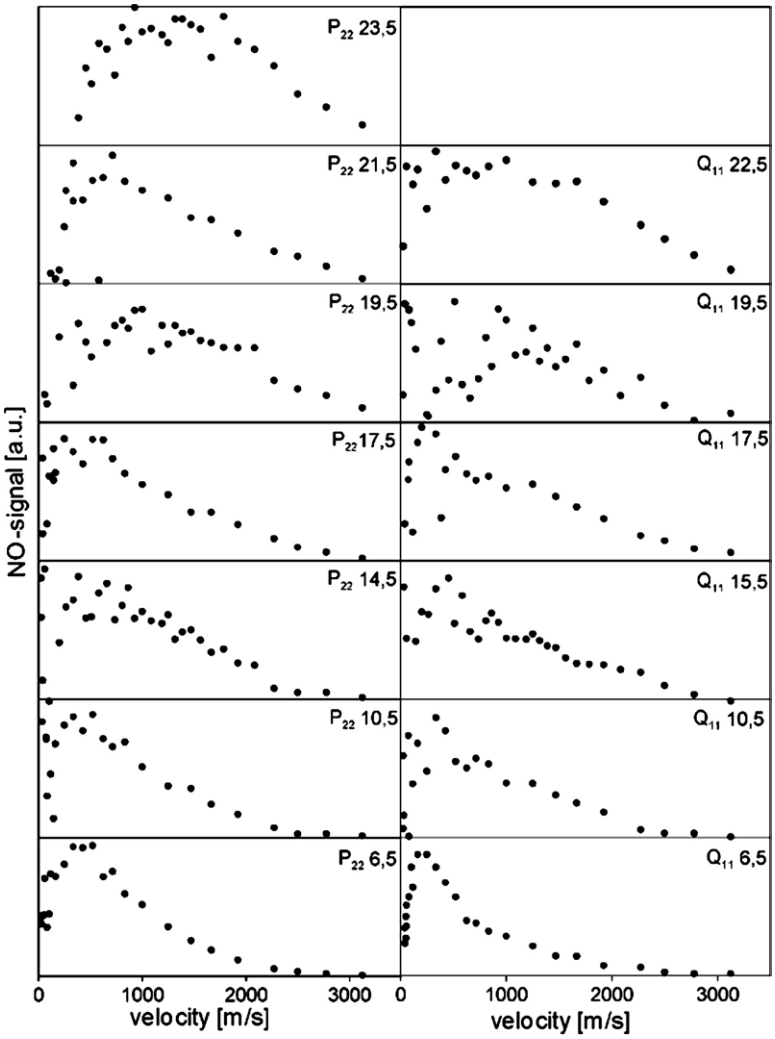

Figure 6. A selected number of velocity flux distributions as a function of rotational quantum number of desorbing NO from Pd aggregates deposited at 300 K with an average size of 45 Å for the $^2\Pi_{1/2}$ (Q_{11} transitions within the REMPI spectra) and the $^2\Pi_{3/2}$ states (P_{22} transitions) [35].

distributions. An increase in desorption efficiency with decreasing aggregate size would therefore be dominated by the amount of such sites available. Particularly small amorphous aggregates with a high degree of defects show efficient desorption. For those aggregates weakly adsorbed species are dominant. This type of reaction path may involve a preceding diffusion from chemisorbed to physisorbed defect adsorption sites. Thermally induced preferential population of weakly bound sites via diffusion from stronger bound regular adsorption sites has been reported for Pd(112) before [88]. One problem arises with this model when trying to explain data for the larger aggregates. While those aggregates still exhibit a substantial number of edges and kinks, the weak adsorbate state is lacking while the laser induced desorption is still observable but is much less efficient.

(2) Laser induced spill over. Laser excitation might also simply induce spill over of NO to the alumina support, causing an increase in the NO population at alumina defect sites. The similar rotational temperatures of NO desorbing from defect states at pure alumina and the alumina modified via Pd aggregates within a large range of aggregates would support this hypothesis. Within this model the increase of desorption efficiency with decreasing aggregate size would simply be a result of a shortening of diffusion paths towards the support. The weakly and more strongly bound molecules are likely to have different diffusion barriers, which would explain the different desorption efficiencies of the two species. Again this explanation leaves experimental findings for the larger aggregates unexplained, which involve a clear drop within rotational temperatures for the largest aggregates.

(3) Electronic effects. It has already been pointed out that charge density variations occur at step sites of metals which extend into the terrace regions. On a nanoparticulate metal thus the whole terrace might be affected, which could lead to drastic changes of properties compared with low index surfaces. Scattering and interference of hot electrons at steps, adsorbates and point defects might thus explain the experimental findings. Such changes in local density with laser excitation could destabilize the NO–surface bond and thus induce either diffusion or desorption.

From the experiments presented none of the above-mentioned processes can be fully ruled out, and further experiments are necessary to finally pinpoint the desorption mechanism.

3.4. Laser induced reactions

3.4.1. CD_4/Pd-nanoparticles/alumina/NiAl(110). Photodissociation has been observed for methane adsorbed at Pd(111), Pt(111) and Cu(111) [89–91]. The question was how the photochemistry is modified when moving to nanosized particles. Figure 7 exhibits TPD data of a saturation coverage of CD_4 adsorbed at palladium nanoparticles of various sizes [34]. The dotted line corresponds to the TPD from Pd(111). The numbers indicated in the spectra are corresponding to the overall amount of palladium deposited according to calibration with a quartz microbalance. The corresponding average particle sizes are given in the figure caption. Molecules with a closed shell adsorb because of van der Waals interactions which are induced via a dynamical response of metal electrons to charge density fluctuations within the adsorbate. Relevant is the charge density close to the Fermi edge of the metal. As this density changes with particle size the adsorbate/nanoparticle decreases with decreasing particle size, as is apparent from maxima shifts within the TPD spectra in figure 7.

3.4.2. Branching between laser induced dissociation and desorption. After UV irradiation with $\lambda = 193$ nm, TPD spectra reveal recombinative desorption of methane at desorption temperatures with a maximum around 140 K (after impinging 1.5×10^{19} photons). Figure 8(a) shows the integrated intensity of the recombinative desorption normalized to the initial intensity of non-dissociated methane as a function of Pd deposited. Figure 8(b) is the relative decrease of non-dissociated methane after UV irradiation for the same preparations. As is apparent, desorption of intact methane molecules is the dominating reaction channel for small palladium particles, while photodissociation may occur when a critical particle size of around 40 Å is exceeded. The efficiency of photodissociation increases by a factor of about ten when increasing the particle size by a factor of two.

If one assumes the same excitation mechanism as on Pd(111), dissociation is induced via the excitation of a mixed state resulting from the antibonding Rydberg state of methane (10 eV above the HOMO for methane in the gas phase) and unoccupied states of the palladium. The

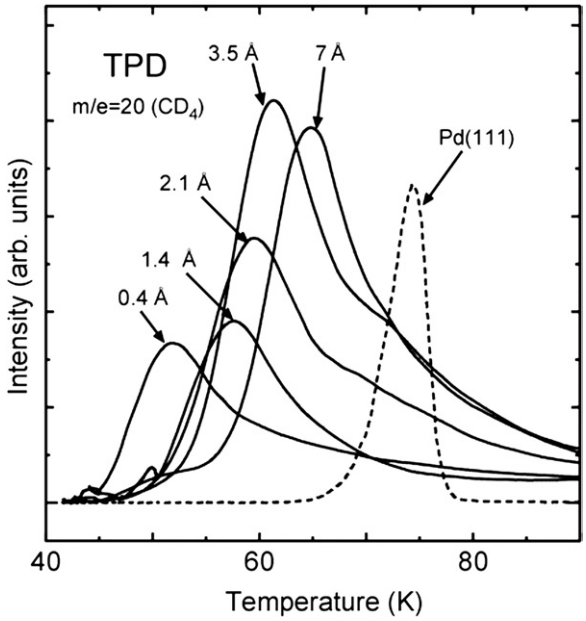

Figure 7. Series of CD_4 TPD spectra (m/z 20; solid curves) of Pd clusters of various sizes deposited on a thin alumina film epitaxially grown on NiAl(110). The sample was exposed to 0.5 L CD_4 at 40 K. The desorption peaks are due to molecular desorption. The numbers denote the total Pd coverages (a deposition of 1.4, 2.1, 3.5 and 7 Å correspond to average aggregate diameters of 37 ± 16, 49 ± 10, 65 ± 10 and 73 ± 10 Å). The dashed curve corresponds to a TPD spectrum of a Pd(111) single-crystal surface after exposure to 0.6 L CD_4 and is depicted in a different scale. Heating rates were 0.5 K s^{-1} for the particles and 0.4 K s^{-1} for the Pd(111) single crystal [34].

delocalization of the metal electrons is important in stabilizing the charge transfer states within this system [92]. An alternative model explains the stabilization of the charge transfer state due to image potential states [93]. In both cases a strong particle size dependence with a concomitant shift of the electronically excited state has to be expected, i.e. for small particles the excitation energy is out of range of the relevant electronic state.

4. Conclusions

From the examples on laser induced processes at nanoparticulate systems it becomes clear that the photochemistry at such systems is rather rich and also rather complex. It is already common knowledge that the chemistry of adsorbates as such might be very different from bulk surface chemistry, a fact which is technologically used in heterogeneous catalysis. However, for the examples presented it becomes clear that apparently kink, edge and defect states which can be found in increasing number with decreasing particle size may influence the photochemistry at nanoparticulate systems to a large extent. Furthermore, the adsorption even for rather weakly adsorbing species is gradually influenced by the particle size. This goes hand in hand with a change of the polarizability which decreases with decreasing particle size. Thus simply the fact alone that the adsorption may be weakened can already change the population of different photochemical reaction pathways. The mean free path of the electrons is also a critical factor. When particles are smaller than this photochemistry starts to be rather efficient. To sum up, one is still rather at the beginning of understanding the photochemistry of supported nanoparticles.

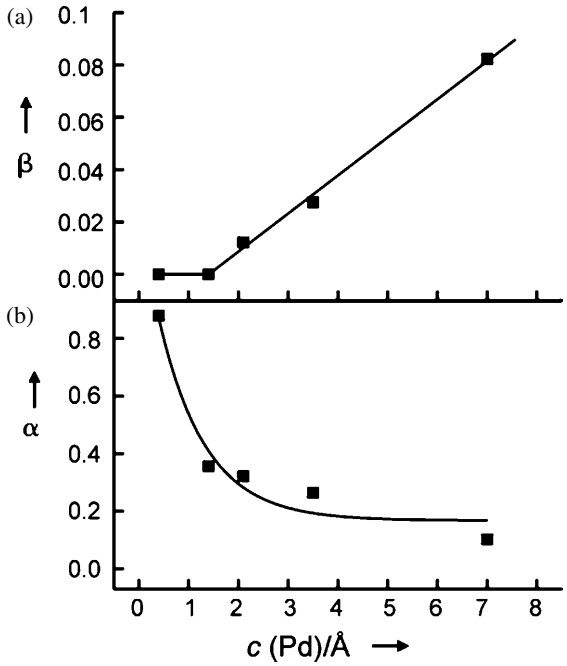

Figure 8. (a) Plot of the CD_3H formation ratio β ($\beta = B/A_0$; B = integrated TPD peak areas of CD_3H after irradiation (recombinative desorption of $CD_3 + H$ (from residual hydrogen adsorption)), A_0 = integrated TPD peak area of initially adsorbed CD_4 before irradiation) as a function of total Pd coverage (corresponding particle diameters see figure 7). (b) Plot of the CD_4 depletion ratio α ($\alpha = 1 - A/A_0$; A_0 as in (a); A = integrated peak areas of CD_4 after irradiation with 1.5×10^{19} photons cm^{-2}) as a function of the total Pd coverage [34].

It is rather challenging and demanding to get the complete picture; however, this will be very rewarding.

Acknowledgments

This work summarizes experimental work from M Kampling, M Wilde, A Wille, St Neuendorf, R Buchwald in cooperation with H-J Freund, Y Matsumoto, K Watanabe, K Fukutani, and Y Murata, to whom the author is very grateful. Discussions with M Bäumer, J Libuda, M Frank and Th Klüner were also very important for this work. D Hoogestraat and B Schroeter-Schuller are gratefully acknowledged for assisting with the layout of the paper. The author would like to further thank the German Science Foundation, the Fonds der Chemischen Industrie and the Land Niedersachsen for financing the experiments.

References

[1] Ho W and Dai H-L (ed) 1993 *Laser Spectroscopy and Photochemistry on Metal Surfaces* (Singapore: World Scientific)
[2] Cavanagh R R, King D S, Stephenson J C and Heinz T F 1993 *J. Phys. Chem.* **97** 786
[3] Al-Shamery K 1996 *Appl. Phys.* A **63** 509
[4] Ho W 1996 *J. Phys. Chem.* **100** 13050
[5] Zhou X L, Zhu X Y and White J 1991 *Surf. Sci. Rep.* **13** 73

[6] Zimmermann F M and Ho W 1995 *Surf. Sci. Rep.* **22** 127
[7] Tanimura K and Ueba H (ed) 2005 *Proc. 10th Int. Workshop on Desorption Induced by Electronic Transitions*; *Surf. Sci.* **593** 1–336
[8] Zare R N 1998 *Science* **279** 1875
[9] Chuang T J 1983 *Surf. Sci. Rep.* **3** 1
[10] Chuang T J, Seki H and Hussla I 1985 *Surf. Sci.* **158** 525
[11] Heidberg J, Noseck U, Suhren M and Weiss H 1993 *Ber. Bunsenges. Phys. Chem.* **97** 329
[12] Redlich B, Zacharias H, Meijer G and von Helden G 2002 *Surf. Sci.* **502/503** 325
[13] Ehrlich D J and Tsao J Y (ed) 1989 *Laser Microfabrication: Thin Film Processes and Lithography* (San Diego, CA: Academic)
[14] Menzel D and Gomer R 1964 *J. Chem. Phys.* **41** 3311
[15] Redhead P A 1964 *Can. J. Phys.* **42** 886
[16] Antoniewicz P R 1980 *Phys. Rev.* B **21** 3811
[17] Wilde M, Fukutani K, Murata Y, Kampling M, Al-Shamery K and Freund H J 1999 *Surf. Sci.* **427/428** 27
[18] Haight R 1983 *Surf. Sci. Rep.* **21** 275
[19] Fauster Th and Steinmann W 1995 Electromagnetic waves: recent developments in research *Photonic Probes of Surfaces* vol 2, ed P Halevi (Amsterdam: Elsevier) pp 347–411
[20] Harris C B, Ge N H, Lingle R L, McNeill J D and Wong C M 1997 *Annu. Rev. Phys. Chem.* **48** 711
[21] Wilde M, Beauport I, Al-Shamery K and Freund H J 1997 *Surf. Sci.* **390** 186
[22] Rezai M A, Stipe B C and Ho W 1999 *J. Chem. Phys.* **110** 4891
[23] Zhdanov V P and Kasemo B 1999 *Surf. Sci. Lett.* **432** L599
[24] Zhdanov V P and Kasemo B 2004 *J. Phys.: Condens. Matter* **16** 7131
[25] Gadzuk J W 1996 *Phys. Rev. Lett.* **76** 4234
[26] Gadzuk J W 1999 *J. Electron. Spectrosc. Relat. Phenom.* **98** 321
[27] Campbell C T 1997 *Surf. Sci. Rep.* **27** 1
[28] Freund H J, Bäumer M, Libuda J, Kuhlenbeck H, Risse T, Al-Shamery K and Hamann H 1998 *Cryst. Res. Technol.* **33** 977
[29] Henry C R 1998 *Surf. Sci. Rep.* **31** 235
[30] Bäumer M and Freund H J 1999 *Prog. Surf. Sci.* **61** 127
[31] Sandell A, Libuda J, Brühwiler P A, Andersson S, Bäumer M, Maxwell J, Mårtensson N and Freund H J 1997 *Phys. Rev.* B **55** 7233
[32] Kreibig U and Vollmer M 1995 *Optical Properties of Metal Clusters* (*Springer Series in Materials Science* vol 25) (Heidelberg: Springer)
[33] Chorkendorff I and Niemantsverdriet J W 2003 *Concepts of Modern Catalysis and Kinetics* (Weinheim: Wiley–VCH)
[34] Watanabe K, Matsumoto Y, Kampling M, Al-Shamery K and Freund H J 1999 *Angew. Chem.* **111** 2328
[35] Kampling M, Al-Shamery K, Freund H J, Wilde M, Fukutani K and Murata Y 2002 *Phys. Chem. Chem. Phys.* **4** 2629
[36] Wille A, Haubitz S and Al-Shamery K 2003 *Chem. Phys. Lett.* **367** 609
[37] Wille A and Al-Shamery K 2003 *Surf. Sci.* **528** 230
[38] Wille A, Buchwald R and Al-Shamery K 2004 *Appl. Phys.* A **78** 205
[39] Carreon M A and Guliants V V 2005 *Eur. J. Inorg. Chem.* **2005** 27
[40] Link S and El-Sayed M A 2003 *Annu. Rev. Phys. Chem.* **54** 331
[41] Burda C, Chen X, Narayanan R and El-Sayed M A 2005 *Chem. Rev.* **10** 1025
[42] Bowker M, Bennett R A, Dickinson A, James D, Smith R D and Stone P 2001 *Stud. Surf. Sci. Catal.* **133** 3
[43] Kralik M and Biffis A 2001 *J. Mol. Catal.* A **177** 113
[44] Thomas J M and Raja R 2001 *Chem. Rec.* **1** 448
[45] Mohr C and Claus P 2001 *Sci. Prog.* **84** 311
[46] Thomas J M, Johnson B F G, Raja R, Sankar G and Midgley P A 2003 *Acc. Chem. Res.* **36** 20
[47] Glass R, Möller M and Spatz J P 2003 *Nanotechnology* **14** 1153
[48] Bradley J S 1994 *Clus. Colloids* 459
[49] Duff D G and Baiker A 1995 *Stud. Surf. Sci. Catal.* **91** 505
[50] Toshima N 1996 *NATO ASI Ser.* 3 **12** 371
[51] Parker A J, Child P A and Palmer R E 2004 *Microelectron. Eng.* **73/74** 542
[52] Nickut P, Tsunoyama H, Sawada T, Matsumoto T, Tsukuda T, Matsumoto Y and Al-Shamery K 2006 in preparation
[53] Boyen H G, Kästle G, Weigl F, Koslowski B, Dietrich C, Ziemann P, Spatz J P, Riethmüller S, Hartmann C, Möller M, Schmid G, Garnier M G and Oelhafen P 2002 *Science* **297** 1533

[54] Avouris P, Lyo I W and Molinàs-Mata P 1995 *Electronic Surface and Interface States on Metallic System* ed E Bertel and M Donath (Singapore: World Scientific) p 217
[55] Stimming U, Vogel R, Kolb D M and Will T 1993 *J. Power Sources* **43** 169
[56] Xirouchaki C and Palmer R E 2004 *Phil. Trans. R. Soc.* A **362** 117
[57] Palmer R E, Sloan P A and Xirouchaki C 2004 *Phil. Trans. R. Soc.* A **362** 1195
[58] Palmer R E, Pratontep S and Boyen H G 2003 *Nat. Mater.* **2** 443
[59] Barabási A L and Stanley H E 1995 *Fractal Concepts in Surface Growth* (Cambridge: Cambridge University Press)
[60] Menges M, Baumeister B, Al-Shamery K, Freund H J, Fischer C and Andresen P 1994 *Surf. Sci.* **316** 103
[61] Libuda J, Bäumer M and Freund H J 1994 *J. Vac. Sci. Technol.* A **12** 2259
[62] Jacobs D C and Zare R N 1986 *J. Chem. Phys.* **85** 5457
[63] Bäumer M, Libuda J and Freund H J 1997 *Chemisorption and Reactivity on Supported Clusters and Thin Film* ed Lambert and Pacchioni (Netherlands: Kluwer–Academic) p 61
[64] Hansen K H, Worren T, Stempel S, Lægsgaard E, Bäumer M, Freund H J, Besenbacher F and Stensgaard I 1999 *Phys. Rev. Lett.* **83** 4120
[65] Wolter K, Seiferth O, Kuhlenbeck H, Bäumer M and Freund H J 1998 *Surf. Sci.* **399** 169
[66] Wolter K, Seiferth O, Libuda J, Kuhlenbeck H, Bäumer M and Freund H J 1998 *Surf. Sci.* **402–404** 428
[67] Ramsier R D, Lee K W and Yates J T 1995 *Surf. Sci.* **322** 243
[68] Wille A, Nickut P and Al-Shamery K 2004 *J. Mol. Struct.* **695/696** 345
[69] Tüshaus M, Berndt W, Conrad H, Bradshaw A M and Persson P 1990 *Appl. Phys.* A **51** 91
[70] Gießel T, Schaff O, Hirschmugl C J, Fernandez V, Schindler K M, Theobald A, Bau S, Lindsey R, Berndt W, Bradshaw A M, Baddeley C, Lee A F, Lambert R M and Woodruff D P 1998 *Surf. Sci.* **406** 90
[71] Sautet P, Rose M K, Duphny J C, Behler S and Salmeron M 2000 *Surf. Sci.* **453** 25
[72] Loffreda D, Simon D and Sautet P 1999 *Surf. Sci.* **425** 68
[73] Kruse Vestergaard E, Thorstrup P, An T, Laegsgaard E, Steensgaard I, Hammer B and Besenbacher F 2002 *Phys. Rev. Lett.* **88** 259601
[74] Hermann K and Bagus P S 1987 *Appl. Phys.* A **44** 63
[75] Wong Y T and Hoffmann R 1991 *J. Phys. Chem.* **95** 859
[76] Bradshaw A M and Hoffmann F M 1978 *Surf. Sci.* **72** 513
[77] Wille A 2004 *PhD Thesis* Oldenburg
[78] Wandelt K 1991 *Surf. Sci.* **251** 387
[79] Szabó A and Yates J T Jr 1995 *J. Chem. Phys.* **102** 563
[80] Komeda T, Kim Y, Kawai M, Persson B N J and Ueba H 2002 *Science* **295** 2055
[81] Misewich J A, Heinz T and Newns D M 1992 *Phys. Rev. Lett.* **68** 3737
[82] Springer C, Head-Gordon M and Tully J C 1994 *Surf. Sci.* **320** L57
[83] Tersoff J and Falicov L M 1981 *Phys. Rev.* B **24** 754
[84] Menges M, Baumeister B, Al-Shamery K, Freund H J, Fischer C and Andresen P 1994 *Surf. Sci.* **316** 103
[85] Beauport I, Al-Shamery K and Freund H J 1996 *Chem. Phys. Lett.* **256** 641
[86] Brown W A and King D A 2000 *J. Phys. Chem.* B **104** 2578
[87] Ramsier R D, Gao Q, Waltenburg H N and Yates J T Jr 1994 *J. Chem. Phys.* **100** 6837
[88] Ramsier R D, Gao Q, Waltenburg H N, Lee K W, Nooij O W, Lefferts L and Yates J T Jr 1994 *Surf. Sci.* **320** 209
[89] Matsumoto Y, Gruzdkov Y A, Watanabe K and Sawabe K 1996 *J. Chem. Phys.* **105** 4775
[90] Watanabe K and Matsumoto Y 1997 *Surf. Sci.* **390** 250
[91] Watanabe K and Matsumoto Y 2000 *Surf. Sci.* **454** 262
[92] Akinaga Y, Taketsugu T and Hrao K 1997 *J. Chem. Phys.* **107** 415
[93] Jennison D R, Stechel E B, Burns A R and Li Y S 1995 *Nucl. Instrum. Methods Phys. Res.* B **101** 22